



OPEN

Corn starch reactive blending with latex from natural rubber using Na⁺ ions augmented carboxymethyl cellulose as a crosslinking agent

Noppol Leksawasdi^{1,2,3}, Thanongsak Chaياس^{1,2}, Pornchai Rachtanapun^{1,2,3}, Sarinthip Thanakkasarnanee^{1,2}, Pensak Jantrawut⁴, Warintorn Ruksiriwanich⁴, Phisit Seesuriyachan^{1,2,3}, Yuthana Phimolsiripol^{1,2,3}, Charin Techapun¹, Sarana Rose Sommano^{5,2}, Toshiaki Ougizawa⁶ & Kittisak Jantanasakulwong^{1,2,3}✉

A mixture of corn starch and glycerol plasticizer (CSG) was blended with latex natural rubber (LNR) and carboxymethyl cellulose (CMC). The addition of 10 phr of CMC improved the Young's modulus (6.7 MPa), tensile strength (8 MPa), and elongation at break (80%) of the CSG/LNR blend. The morphology of the CSG/LNR/CMC blends showed a uniform distribution of LNR particles (1–3 μm) in the CSG matrix. The addition of CMC enhanced the swelling ability and water droplet contact angle of the blends owing to the swelling properties, interfacial crosslinking, and amphiphilic structure of CMC. Fourier transform infrared spectroscopy confirmed the reaction between the C=C bond of LNR and the carboxyl groups (–COO[–]) of CMC, in which the Na⁺ ions in CMC acted as a catalyst. Notably, the mechanical properties of the CSG/LNR/CMC blend were improved owing to the miscibility of CSG/CMC and the CMC/LNR interfacial reaction. The CSG/LNR/CMC biodegradable polymer with high mechanical properties and interfacial tension can be used for packaging, agriculture, and medical applications.

Biodegradable polymers have attracted considerable attention because they are environmentally friendly and readily degradable. They can be particularly competitive in certain sectors of the plastics market, such as food packaging^{1,2} at both the industrial and street food levels, where hygiene must be practiced to prevent packaging contamination³. Petroleum-based polymers generated from petroleum resources subject to depletion have detrimental effects on the environment^{4,5}. Therefore, biodegradable polymers are being widely investigated to replace petroleum polymers, with examples including polylactic acid (PLA)^{6,7}, polybutylene succinate (PBS)^{8,9}, thermoplastic starch (TPS)¹⁰, chitosan^{11,12}, pectin^{13–15}, polysaccharides^{16,17}, keratin¹⁸, and fibroin¹⁹.

Starch is a natural polymer possessing desirable traits such as complete biodegradability, low cost, and renewability. Starch is produced from plants that are widely consumed by humans. Starch is a semi-crystalline biopolymer whose structure contains starch granules with different amylose/amylopectin ratios, depending on the starch resources and gelling properties of water and heat²⁰. Starch processing involves chemical reactions, including melting, gelatinization, and water diffusion²¹. Some common resources for the production of starch have been investigated, such as cassava²², mung beans²³, and corn²⁴, along with the development of special enzymes that can

¹School of Agro-Industry, Faculty of Agro-Industry, Chiang Mai University, Mae Hia, Muang, Chiang Mai, Thailand. ²Cluster of Agro Bio-Circular-Green Industry, Faculty of Agro-Industry, Chiang Mai University, Mae Hia, Muang, Chiang Mai, Thailand. ³Center of Excellence in Materials Science and Technology, Faculty of Science, Chiang Mai University, Mae Hia, Muang, Chiang Mai, Thailand. ⁴Department of Pharmaceutical Sciences, Faculty of Pharmacy, Chiang Mai University, Mae Hia, Muang, Chiang Mai, Thailand. ⁵Plant Bioactive Compound Laboratory (BAC), Department of Plant and Soil Sciences, Faculty of Agriculture, Chiang Mai University, Mae Hia, Muang, Chiang Mai, Thailand. ⁶Department of Chemistry and Materials Science, Tokyo Institute of Technology, Meguro-ku, Tokyo, Japan. ✉email: kittisak.jan@cmu.ac.th

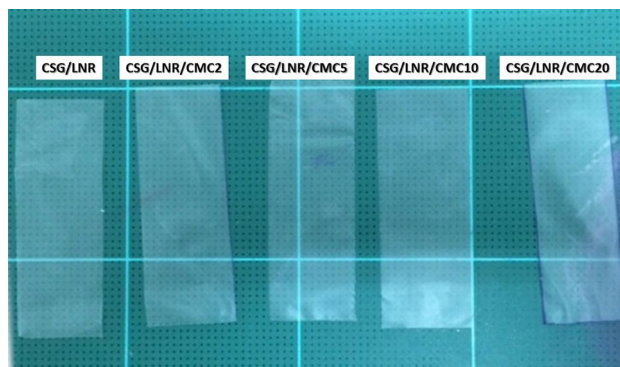


Figure 1. Image of CSG/LNR films blending with CMC 0, 2, 5, 10, 20 phr.

degrade starch under harsh conditions²⁵. Corn starch (CS) is the world's largest starch resource²⁶ and is widely used in food processing²⁷ and food packaging²⁸.

Natural rubber (NR) is composed of *cis*-1-*s*-polyisoprene, which is extracted from the para rubber tree (*Hevea brasiliensis*) to obtain latex²⁹. This latex from NR (LNR) has a relatively high water content and up to 60% rubber content. LNR contains rubber particles, lipids, carbohydrates, and proteins in aqueous solution. Skim latex is purified using a creaming agent and saponification³⁰. Ammonia is a common chemical used to prevent coagulation and bacterial growth in LNR³¹. Because of its excellent properties, LNR is used extensively to manufacture several products (e.g., gloves, balloons, rubber boots, and condoms). The mechanical properties of rubber are improved by crosslinking in the rubber phase³². LNR is also the main natural polymer resource of the global agricultural economy³³; however, NR prices have dropped because of economic conditions³⁴. There have been some studies on NR blending utilizing starch³⁵. The mechanical properties of NR blends can be improved by crosslinking certain functional groups in rubber using various methods³⁶.

Carboxymethyl cellulose (CMC) is a cellulose derivative obtained from alkali cellulose and sodium salt reactions³⁷. The main applications of CMC include food, paper, printing, medicine, and packaging³⁸. CMC contains carboxylic groups with Na⁺ ions³⁹ and exhibits high viscosity and nontoxic properties. CMC has been prepared using various source materials such as asparagus⁴⁰, palm bunches⁴¹, bacterial cellulose^{42,43}, and chitosan⁴⁴. CMC can also act as a compatibilizer to improve the properties of starch⁴⁵. The mechanical properties of CMC/natural rubber blends with polyaniline⁴⁶ and cellulose⁴⁷ have been previously reported. Azura et al. presented the interaction between nano-starch filler and LNR, which could improve the mechanical properties of the blends⁴⁸. However, few studies have investigated the improvement in the mechanical properties of starch blended with NR undergoing a reaction with CMC.

The aim of this study was therefore to develop biopolymer films with good mechanical properties using reactive blending of CS and glycerol (CSG), LNR, and CMC. CS was selected as the main matrix for the blend because of its biodegradability, high purity, chemical modification abilities, low cost, and abundance. Glycerol was used as a plasticizer to improve the flexibility and processing ability of the CS. LNR was blended with CSG to enhance the toughness and flexibility as an elastic phase of the blends. CMC was used as a crosslinking agent. It was suggested that the high compatibility of CS/CMC and the reaction between CMC and LNR would improve the mechanical properties of the blends. A tough, transparent, water-resistant biodegradable material with high tensile properties was developed. The effects of CMC addition and the presence of Na⁺ ions in the CMC were investigated. The tensile properties, morphology, water resistance, and reaction mechanisms were also evaluated, resulting in a high tensile strength biomaterial made from a starch/natural rubber blend for packaging, agriculture, and medical applications.

Results and discussions

Reaction mechanism. CS with glycerol plasticizer (CSG) was blended with CMC and LNR through solution mixing at 80 °C for 1 h. The mixed solutions were applied to films and dried at 60 °C for 24 h. Images of the CSG/LNR blend with CMC 0–20 phr samples are shown in Fig. 1. The reaction mechanisms of CSG, CMC, and LNR were investigated using FTIR spectroscopy. Figure 2a shows the FTIR spectra of CMC, CSG, and CSG/LNR blends with 0–20 phr CMC. The FTIR spectra of LNR (*cis*-1,4 polyisoprene) exhibited C–H stretching (2960, 2927, and 2852 cm⁻¹), C=C stretching (1661 cm⁻¹), C–H deformation of stretching –CH₂– (1448 cm⁻¹), C–H deformation of –CH₃ (1376 cm⁻¹), and C=C–H (835 cm⁻¹)^{49,50}. The CSG spectra exhibited peaks at 1643 (–OH bending), 1016, and 929 cm⁻¹ (–CO stretching)^{51,52}. The CMC spectra exhibited peaks at 3040 (–OH stretching), 2897 (–CH stretching), 1602 (COO⁻), and 1427 cm⁻¹ (COO⁻Na⁺)^{53,54}. The spectra of the CSG/LNR blend exhibited a combination of the individual CSG and LNR spectra. The CSG/LNR/CMC blend presented an increase in peak intensities at 1602 (COO⁻) and 1427 cm⁻¹ (COO⁻Na⁺) of CMC. To study the reaction mechanism of the blend, the LNR phase was extracted from the CSG/LNR and CSG/LNR/CMC blends. The spectra of CSG, CMC, LNR, and the extracted LNR are shown in Fig. 2b. The CH₂– peak at 1448 cm⁻¹ of the LNR was used to normalize the extracted LNR samples. The extracted LNR from the CSG/LNR exhibited spectra similar to those of pure LNR, with peaks at 1661 (C=C stretching) and 835 cm⁻¹ (C=C–H). Furthermore, in the LNR extracted from the CSG/LNR/CMC blend, the peak at 1661 cm⁻¹ (C=C) shifted to 1657 cm⁻¹ and increased in

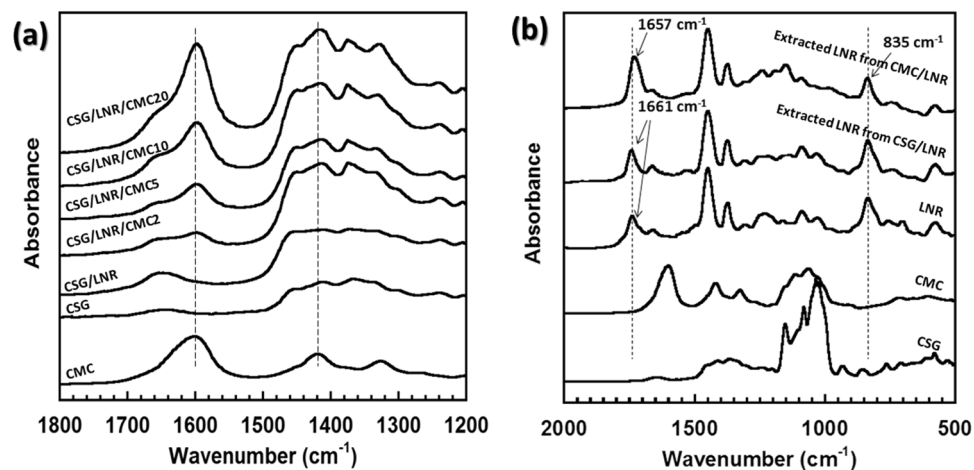


Figure 2. FTIR spectra of (a) CMC, CSG, CSG/LNR blend with CMC 0–20 phr at 1200–1800 cm^{-1} , and (b) CSG, CMC, LNR, and the extracted LNR from CSG/LNR and CMC/LNR. at 500–2000 cm^{-1} .

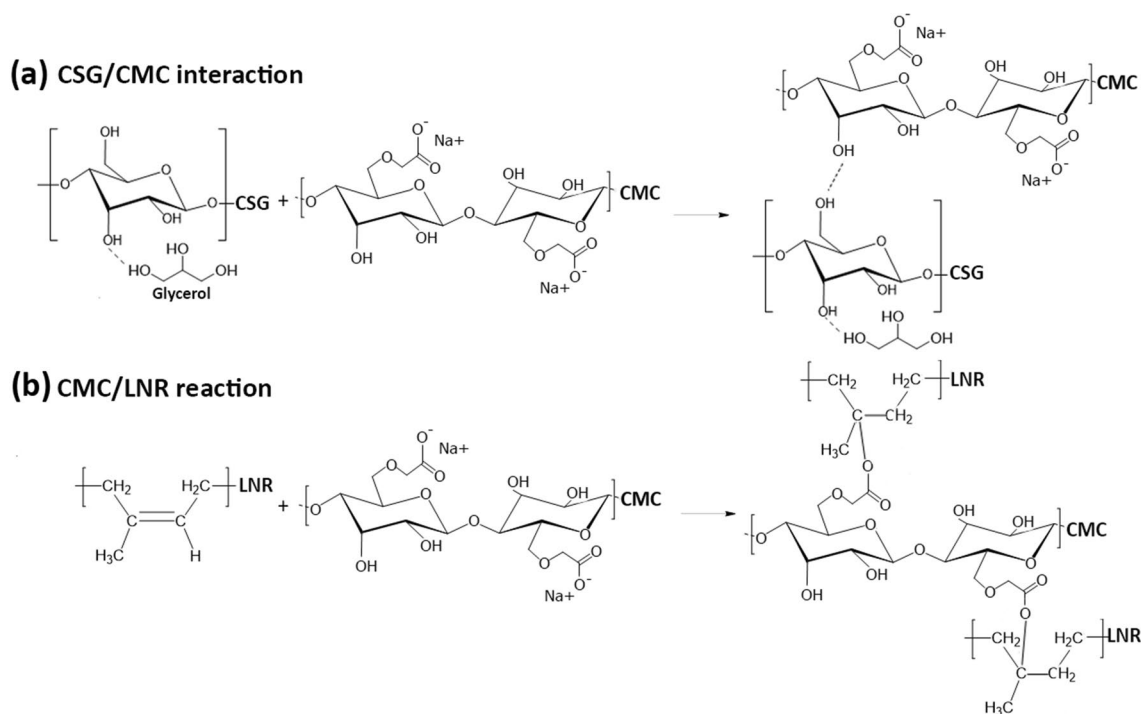


Figure 3. Suggested reaction of (a) interaction between CSG and CMC and (b) reaction between CMC and LNR.

intensity. This indicates a new $\text{C}-\text{O}$ peak due to the reaction between CMC and LNR. The intensity of the peak at 835 cm^{-1} ($\text{C}=\text{C}-\text{H}$) decreased compared to that of pure LNR owing to the reduction of the $\text{C}=\text{C}-\text{H}$ structure in the LNR chain. The Na^+ ion in CMC is in the form of a Lewis acid catalyst⁵⁵. Crosslinking at the $\text{C}=\text{C}$ structure of LNR was accelerated by the Lewis acid catalyst, as reported previously⁵⁶. Supanakorn et al.⁴⁷ confirmed the interaction between CMC and LNR, which improved the mechanical properties of the LNR/cellulose/CMC blend. It has also been reported that Na^+ ions inside the CMC accelerate the reaction through its COO^- groups⁴⁵. It was confirmed that the $\text{C}=\text{C}$ of the LNR structure reacted with the COO^- of CMC as the Na^+ ion in CMC acted as a catalyst. The suggested reaction mechanism is illustrated in Fig. 3. CSG showed high compatibility with CMC owing to their structural similarity and interaction between the $-\text{OH}$ groups (Fig. 3a), whereas a reaction occurred between the $\text{C}=\text{C}$ of LNR and COO^- of CMC (Fig. 3b).

Mechanical properties. Figure 4 shows the stress–strain curves of the CSG/LNR blends with 0–20 phr CMC. The Young’s modulus was calculated from the slope at the early stage of the stress–strain curve. The CSG/

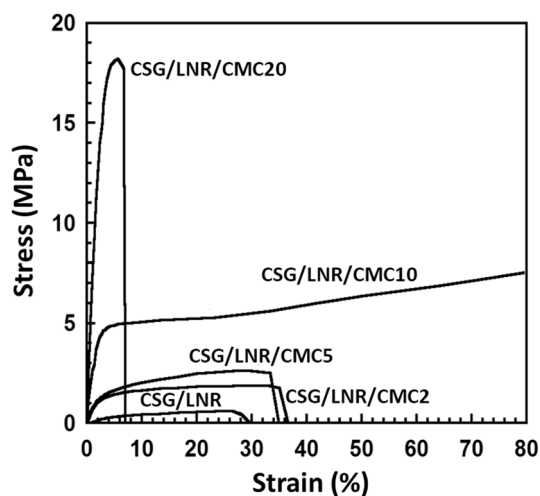


Figure 4. Tensile stress–strain curves of the CSG/LNR blends with CMC of 0, 2, 5, 10, and 20 phr ($n = 5$).

Sample	Young's modulus (MPa)	Maximum tensile strength (MPa)	Elongation at break (%)
CSG/LNR	0.3 ± 0.08^a	0.5 ± 0.08^a	30.1 ± 2.40^b
CSG/LNR/CMC2	2.4 ± 0.07^b	1.7 ± 0.12^b	35.4 ± 2.89^c
CSG/LNR/CMC5	2.8 ± 0.08^c	2.9 ± 0.21^c	33.3 ± 3.21^c
CSG/LNR/CMC10	6.7 ± 0.08^d	8.0 ± 0.43^d	79.9 ± 4.35^d
CSG/LNR/CMC20	18.2 ± 0.08^e	18.0 ± 2.1^e	7.80 ± 0.51^a

Table 1. Young's modulus, maximum tensile strength, and elongation at break of CSG/LNR blends with 0–20 phr CMC. Means with different lowercase superscript letters in the same column are significantly different ($P < 0.05$).

LNR blend showed a low Young's modulus of 0.3 MPa, a maximum tensile strength of 0.5 MPa, and an elongation at break of 30% (Table 1). The addition of CMC resulted in an increase in Young's modulus and maximum tensile strength. The CSG/LNR/CMC10 blend exhibited a Young's modulus of 6.7 MPa, a maximum tensile strength of 8 MPa, and an elongation at break of 80%, with all values higher than those for the blends where CMC was added at 0, 2, and 5 phr. The CSG/LNR/CMC20 blend exhibited the highest Young's modulus (18.2 MPa) and maximum tensile strength (18 MPa) and the lowest elongation at break because of the high interfacial crosslinking density, reaction mechanism, and high mechanical properties of CMC. The tensile strength, elongation at break, and toughness of the CSG/LNR blend were improved by adding CMC, particularly for the CSG/LNR/CMC10 sample compared to the CSG/LNR blend. The toughness of the sample is related to the area under the stress–strain curve⁵⁷. The Young's modulus of starch increased with the CMC content⁵⁸, and a high interfacial reaction improved the mechanical properties of the polymer blends, which has been reported previously⁵⁹. An improvement in the mechanical properties of natural rubber by the addition of CMC has also been reported^{46,47}. CMC was found to improve the interfacial adhesion between CSG and LNR through CMC crosslinking as a compatibilizer. CMC is compatible with starch, carboxylic groups, and sodium ions in its structure⁴⁵. These induced the formation of crosslinking between CSG and LNR through CMC. CMC acted as a physical crosslinking point to connect the structures of starch and rubber together, which provided the combined properties of CSG, CMC, and LNR. In the CSG/LNR/CMC sample, CMC 10% was suitable for connecting CSG (hard phase) and LNR (elastic phase), providing high elongation at breaking. In the CSG/LNR/CMC20 sample, high content, mechanical properties, and physical crosslinking of CMC increased the tensile strength and brittleness of the blend. The improvement in the tensile properties was attributed to the compatibility of CSG/CMC and the occurrence of the interfacial crosslinking density of CMC/LNR through a reaction mechanism between the C=C of LNR and COO⁻ of CMC (Fig. 3b).

Morphology. The morphologies of the samples were observed using SEM. The samples were broken in liquid nitrogen, and then the LNR phase on the fracture surfaces was extracted by immersion in toluene at 60 °C for 1 h. Figure 5 shows the fracture surface images of the CSG/LNR and CSG/LNR/CMC blends with 2, 5, 10, and 20 phr of CMC. The CSG/LNR blend exhibited voids representing the LNR particles extracted using toluene because NR dissolves in toluene⁶⁰. ImageJ software was used to evaluate the rubber particle sizes. The LNR particle sizes in the CSG/LNR blend were 1–3 μm. The addition of CMC at 2, 5, 10, and 20 phr resulted in the dispersion of the LNR rubber particles (1–3 μm) in the CSG matrix. The LNR formed small rubber particles in

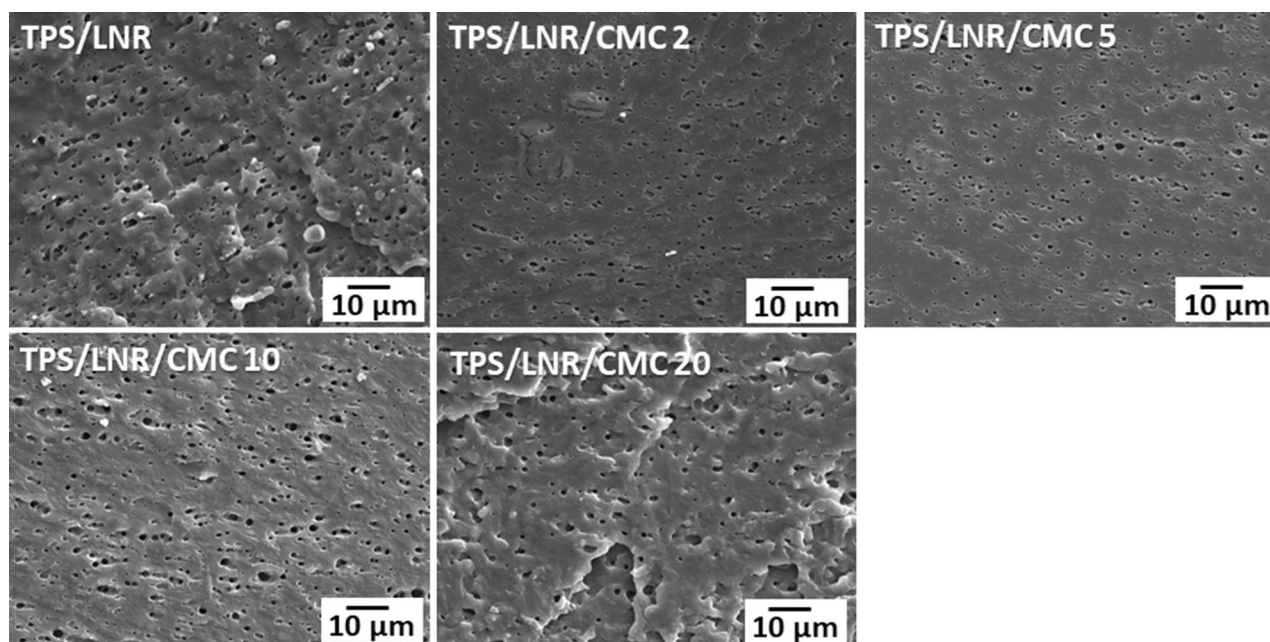


Figure 5. SEM images of CSG/LNR blends with CMC 0, 2, 5, 10, and 20 phr.

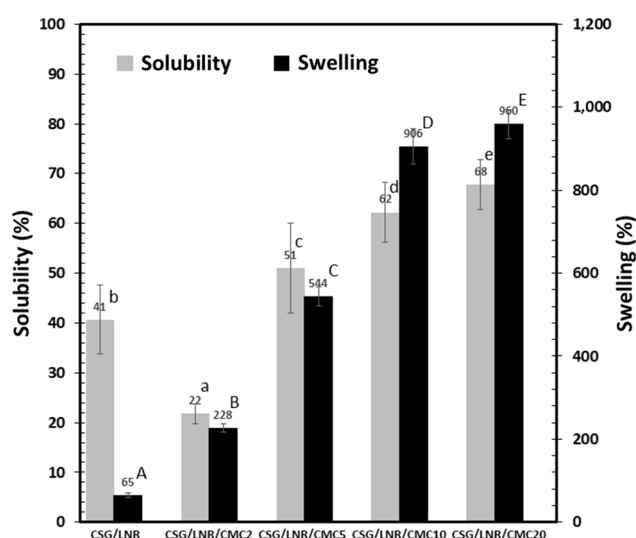


Figure 6. Solubility and swelling of the CSG/LNR/CMC blends with 0, 2, 5, 10, and 20 phr of CMC ($n=5$). Means with different lowercase letters of solubility and uppercase letters of solubility are significantly different ($P < 0.05$).

the CSG matrix, while the addition of CMC did not reduce the particle size of the LNR. The improvement in the tensile properties was probably due to the high tensile properties of CMC, interfacial crosslinking density of CSG/LNR, and crosslinking density inside the LNR phase.

Solubility and swelling. The solubility and swelling of the samples were measured by immersing the samples in distilled water at 25 °C for 24 h. The CSG film was prepared by the controlled mixing of starch with glycerol (70/30%w/w). The solubility and swelling degree of the CSG/LNR film were 41% and 65%, respectively (Fig. 6). Solubility was calculated from the weight loss of the samples in water. The solubility of CSG/LNR/CMC2 decreased to 22% owing to the formation of interfacial crosslinking density between CMC and LNR. The elevated CMC content increased the solubility of the CSG/CMC/LNR blends because of the high soluble material content in the blends. The CSG/LNR showed low swelling owing to the low crosslinking density between the CSG and LNR phases. The degree of swelling increased with the CMC content due to the increase in the interfacial crosslink density of CSG/LNR through the CMC reaction mechanism (Fig. 2), and the crosslinking inside the CMC phase through Na^+ ions. The CMC structure contains Na^+ ions from its synthesis process, which form physical crosslinking with the COOH groups of CMC⁶¹. CS is a hydrophilic material⁶², whereas CMC

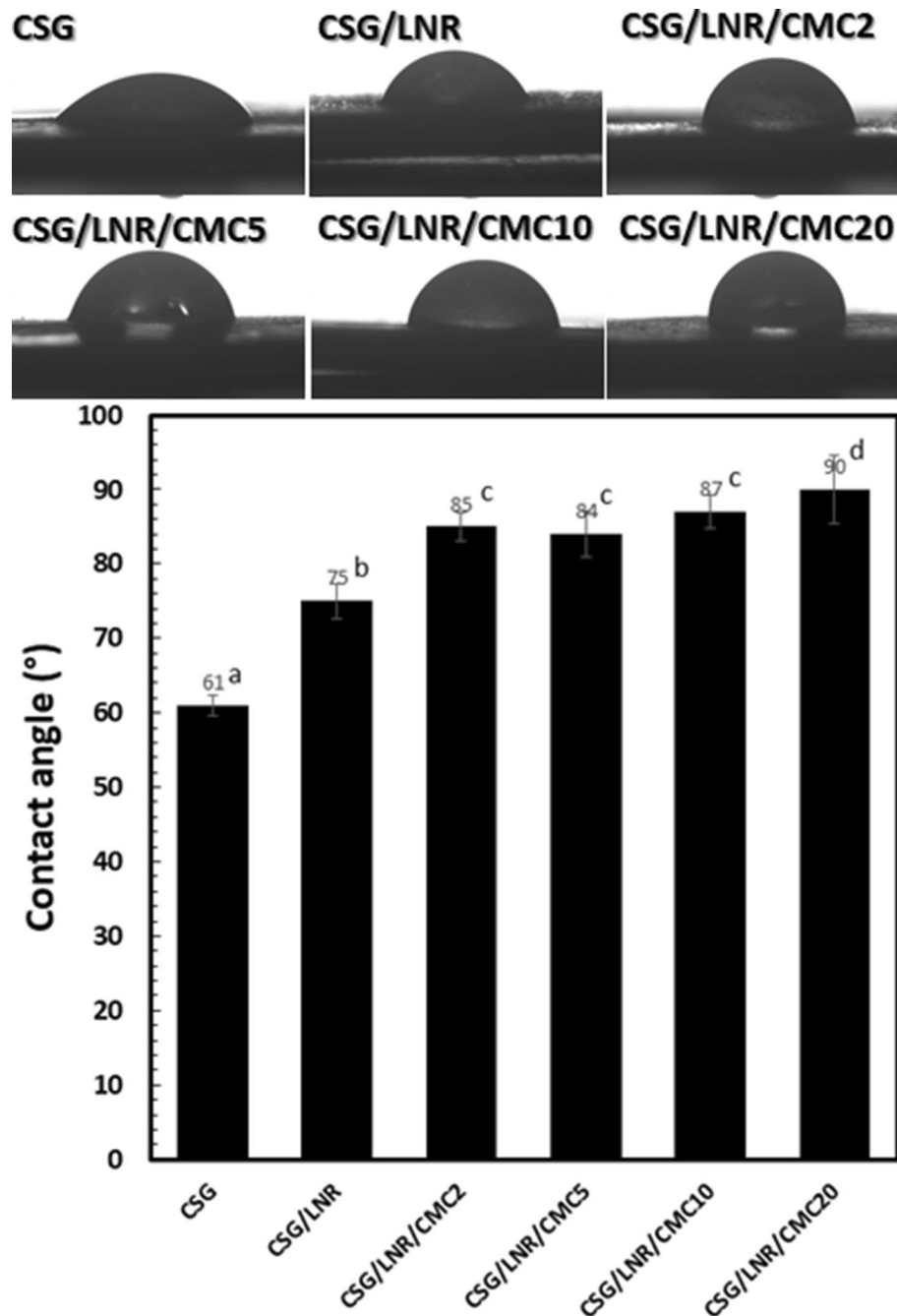


Figure 7. Contact angles of CSG and the CSG/LNR blends with 0, 2, 5, 10, and 20 phr of CMC at 3 min (n=5). Means with different lowercase superscript letters are significantly different ($P < 0.05$).

forms a gel in water^{37,41}. The increase in the swelling degree was evidence of the hydrophilic properties of CS and CMC^{62,63}, the swelling ability of CMC⁶⁴, and the interfacial crosslinking density of CSG/LNR through the CMC reaction mechanism.

Contact angle. The water droplet contact angle is related to the hydrophilicity, crosslinking, and surface tension of the materials. Figure 7 shows the contact angle of CSG and the CSG/LNR blends with 0–20 phr of CMC at 3 min. CSG exhibited a low contact angle of 61°. The contact angle of the CSG/LNR blends increased with increasing CMC content, especially at 20 phr. CS is a polar material, whereas amphiphilic CMC combines polar and nonpolar structures⁶³. The increase in the contact angle of the CSG/LNR blend was probably caused by small hydrophobic rubber particles that were finely dispersed in the CSG matrix. The increase in the contact angle of CSG/LNR/CMC2 may be due to the combination of the interfacial crosslinking density between LNR and CMC, hydrophobicity of LNR, and the non-polar portion of CMC. Particles of hydrophobic LNR with a

Sample	CSG (wt%)	LNR (wt%)	CMC (phr/CSG)
CSG/LNR	90	10	–
CSG/LNR/CMC2	90	10	2
CSG/LNR/CMC5	90	10	5
CSG/LNR/CMC10	90	10	10
CSG/LNR/CMC20	90	10	20

Table 2. Designation and formulation of the CSG/LNR/CMC blends.

crosslinked phase through CMC increased the interfacial tension and repelled the water droplet from the surface. The addition of 5–20 phr of CMC increased the contact angle to 85–90°, owing to the enhanced non-polar portion of CMC and interfacial crosslinking density.

Conclusions

A new biopolymer film with improved mechanical properties and interfacial tension was successfully developed by blending CSG with CMC and LNR. The incorporation of CMC into the CSG/LNR blend enhanced the tensile properties of the blend because of the improvement in the interfacial reaction, miscibility of CSG/CMC, LNR crosslink, and mechanical properties of CMC. The interfacial crosslinking density of CMC/LNR improved the solubility of the CSG/CMC/LNR blend. The swelling properties were enhanced with CMC content owing to the gel formation of CMC. The contact angle increased with the CMC content owing to the hydrophobic nature of LNR, interfacial crosslinking density of CMC/LNR, and non-polar structural portion of the amphiphilic CMC. The FTIR results confirmed the reaction between the COO[−] groups of CMC and the C=C groups of LNR in the presence of Na⁺ ions acting as Lewis acid catalysts. This reaction mechanism and the compatibility of CSG/CMC improved the mechanical properties and interfacial tension of the CSG/CMC/LNR blend. The CSG/CMC/LNR blend, with its excellent properties, can be used in packaging, agriculture, and medical applications.

Methods

Materials. CS (Super-Find brand with MW of 2.54×10^8 g/mol) was procured from R&B Food Supply Public Co. Ltd., Bangkok, Thailand. Glycerol (99%) was procured from Yok Inter Trade (Chiang Mai) Co. Ltd., Chiang Mai, Thailand. Food grade CMC (FVH6-3, DS = 0.65–0.85) was procured from Guoyu Environmental S&T Co. Ltd., Changzhou, Jiangsu, China. LNR (Mastex brand) was procured from Mastex Co. Ltd., Nakornpathom, Thailand.

Sample preparation. CS and glycerol (CSG) were mixed at a ratio of 70/30 (% w/w) with distilled water (50 g/100 mL) through agitation in a water bath at 80 °C for 30 min. CMC was dissolved in distilled water (1 g/10 mL) at 80 °C for 10 min. LNR was incorporated into the CSG solution during the mixing process, followed by the addition of CMC solution. The concentration of CMC was added at 2–20 phr (parts/hundred) of CSG. The formulations of the CSG/LNR/CMC blends are listed in Table 2. The solutions were cast on a clean glass plate and then dried in a hot-air oven at 60 °C for 24 h.

Tensile properties. The tensile properties of the samples were evaluated in quintuplicate using a tensile tester (Tensilon UTM-II-20; Orientec Co. Ltd., Tokyo, Japan) at a crosshead speed of 2 mm/min. Bone-shaped samples were prepared using a die-cutting mold with gauge lengths, widths, and thicknesses of 10, 3, and 0.2 mm, respectively.

Scanning electron microscopy. Morphological images of the samples were obtained using scanning electron microscopy (SEM; SM-200, Topcon Corp., Tokyo, Japan). The samples were broken in liquid nitrogen prior to the extraction of the fractured surfaces of the rubber phase using toluene at 60 °C for 1 h. The extracted fractured surfaces of the samples were coated with a thin layer of gold and measured at an acceleration voltage of 10 kV. The particle sizes of the rubber were calculated using the ImageJ software.

Swelling measurement. The swelling percentage of the samples in water was measured for a specimen size of 50 mm × 50 mm × 0.05 mm (width × length × thickness). The samples were dried at 60 °C for 24 h and soaked in 50 mL of distilled water at 25 °C for 24 h. The swelling ratio was averaged over five samples using Eq. (1)⁶⁵.

$$\text{Swelling ratio(\%)} = \frac{W_a - W_b}{W_b} \times 100 \quad (1)$$

where W_a is the swollen weight and W_b is the dried weight.

Solubility measurement. The sample size was 50 mm × 50 mm × 0.05 mm (width × length × thickness). The sample films were dried at 60 °C for 24 h and placed in a 250 mL Erlenmeyer flask containing 50 mL of distilled water. The samples were shaken at 25 rpm for 24 h using a shaker (OS-300, Hysc Lab, Scilution Co. Ltd.,

Nonthaburi, Thailand). The supernatant was filtered and the remaining samples were collected. The residue on the filter paper was dried in a hot-air oven at 80 °C for 24 h. The water solubility percentage was calculated in quintuplicate using Eq. (2)⁶⁶.

$$\text{Solubility (\%)} = \frac{W_1 - W_2}{W_1} \times 100 \quad (2)$$

where W_1 is the initial weight and W_2 is the dried weight of the filtered sample.

Contact angle. Drop shape analysis (DSA30E, Kruss Co. Ltd., Hamburg, Germany) was used to observe the water droplet contact angle. Samples were prepared by casting on a clean glass plate. Water was dropped onto the surface of the samples before recording the images at 3 min. Five samples were obtained for each condition.

Fourier transform infrared spectrometer (FTIR). FTIR (FT/IR-480 plus, Jasco Corp., Japan) was used to observe the reactions in the CSG/LNR/CMC blends. The samples were prepared as thin films using the solution-casting method. The measurement was performed from 600 cm^{-1} to 4000 cm^{-1} with a resolution of 4 cm^{-1} .

Statistical analysis. One-way ANOVA using SPSS software was used to analyze the results. Statistically significant differences at a confidence interval of 95% ($P < 0.05$) were estimated using Duncan's test over five samples.

Received: 21 July 2021; Accepted: 7 September 2021

Published online: 28 September 2021

References

- Filiciotto, L. & Rothenberg, G. Biodegradable plastics: Standards, policies, and impacts. *Chemoschem* **14**, 56–72 (2021).
- Ncube, L. K., Ude, A. U., Ogunmuyiwa, E. N., Zulkifli, R. & Beas, I. N. Environmental impact of food packaging materials: A review of contemporary development from conventional plastics to polylactic acid based materials. *Materials (Basel)* **13**(21), 4994 (2020).
- Trafialek, J. *et al.* Street food vendors' hygienic practices in some Asian and EU countries—A survey. *Food Control* **85**, 212–222 (2018).
- Capezza, A. *et al.* Acylation of agricultural protein biomass yields biodegradable superabsorbent plastics. *Commun. Chem.* **4**, 52 (2021).
- Yates, M. & Berlow, C. Y. Life cycle assessments of biodegradable, commercial biopolymers—A critical review. *Resour. Conserv. Recycl.* **78**, 54–66 (2013).
- Jantanasakulwong, K., Kobayashi, Y., Kuboyama, K. & Ougizawa, T. Thermoplastic vulcanizate based on poly(lactic acid) and acrylic rubber blended with ethylene ionomer. *J. Macromol. Sci. Part B* **55**(11), 1068–1085 (2016).
- Kiattipornpithak, K. *et al.* Reaction mechanism and mechanical property improvement of poly(lactic acid) reactive blending with epoxy resin. *Polymers* **13**(15), 2429 (2021).
- Fenni, S. E. *et al.* Crystallization and self-nucleation of PLA, PBS and PCL in their immiscible binary and ternary blends. *Thermochim. Acta* **667**, 117–130 (2019).
- Jantanasakulwong, K., Rohindra, D., Mori, K., Kuboyama, K. & Ougizawa, T. Thermoplastic elastomer by reactive blending of poly(butylene succinate) with ethylene-propylene-diene terpolymer and ethylene-1-butene rubbers. *J. Elastomers Plast.* **47**(3), 215–231 (2015).
- Jantanasakulwong, K. *et al.* Effect of dip coating polymer solutions on properties of thermoplastic cassava starch. *Polymers* **11**(11), 1746 (2019).
- Jantanasakulwong, K. *et al.* Reactive blending of thermoplastic starch, epoxidized natural rubber and chitosan. *Eur. Polym. J.* **84**, 292–299 (2016).
- Rachtanapun, P. *et al.* Characterization of chitosan film incorporated with curcumin extract. *Polymers* **13**(6), 963 (2021).
- Jantrawut, P., Chambin, O. & Ruksiriwanich, W. Scavenging activity of rutin encapsulated in low methoxyl pectin beads. *Cellul. Chem. Technol.* **49**, 51–54 (2015).
- Chaiwarit, T., Ruksiriwanich, W., Jantanasakulwong, K. & Jantrawut, P. Use of orange oil loaded pectin films as antibacterial material for food packaging. *Polymers* **10**(10), 1144 (2018).
- Wongkaew, M., Sommano, S. R., Tangpao, T., Rachtanapun, P. & Jantanasakulwong, K. Mango peel pectin by microwave-assisted extraction and its use as fat replacement in dried chinese sausage. *Foods* **9**(4), 450 (2020).
- Surin, S. *et al.* Optimization of ultrasonic-assisted extraction of polysaccharides from purple glutinous rice bran (*Oryza sativa* L.) and their antioxidant activities. *Sci. Rep.* **10**, 10410 (2020).
- Chaisuwan, W. *et al.* Microbial exopolysaccharides for immune enhancement: Fermentation, modifications and bioactivities. *Food Biosci.* **35**, 100564 (2020).
- Kaewsalud, T. *et al.* Biochemical characterization and application of thermostable-alkaline keratinase from *Bacillus halodurans* SW-X to valorize chicken feather wastes. *Waste Biomass Valorization* **12**, 3951–3964 (2020).
- Yakul, K. *et al.* Enzymatic valorization process of yellow cocoon waste for production of antioxidative sericin and fibroin film. *J. Chem. Technol. Biotechnol.* **96**(4), 953–962 (2021).
- Wang, B. *et al.* Structural changes in corn starch granules treated at different temperatures. *Food Hydrocolloids* **118**, 106760 (2021).
- Liu, H., Xie, F., Yu, L., Chen, L. & Li, L. Thermal processing of starch-based polymers. *Progress Polymer Sci.* **34**(12), 1348–1368 (2009).
- Engel, J. B., Luchese, C. L. & Tessaro, I. C. How are the properties of biocomposite foams influenced by the substitution of cassava starch for its residual sources?. *Food Hydrocolloids* **118**, 106790 (2021).
- Rachtanapun, P. *et al.* Thermoplastic mung bean starch/natural rubber/sericin blends for improved oil resistance. *Int. J. Biol. Macromol.* **188**(1), 283–289 (2021).
- Wang, J., Jiang, X., Guo, Z., Zheng, B. & Zhang, Y. Insights into the multi-scale structural properties and digestibility of lotus seed starch-chlorogenic acid complexes prepared by microwave irradiation. *Food Chem.* **361**, 130171 (2021).
- Takenaka, S. *et al.* Characterization of the native form and the carboxy-terminally truncated halotolerant form of α -amylases from *Bacillus subtilis* strain FP-133. *J. Basic Microbiol.* **55**(6), 780–789 (2015).
- Sarka, E. & Dvoracek, V. New processing and applications of waxy starch [A review]. *J. Food Eng.* **206**, 77–87 (2017).
- Warren, F. J., Gidley, M. J. & Flanagan, B. M. Infrared spectroscopy as a tool to characterise starch ordered structure—a joint FTIR–ATR, NMR XRD and DSC study. *Carbohydr. Polymer* **139**, 35–42 (2016).

28. Homsaard, N. *et al.* Efficacy of cassava starch blending with gelling agents and palm oil coating in improving egg shelf life. *Int. J. Food Sci. Technol.* **56**(8), 3655–3661 (2021).
29. Long, X., Fang, Y., Qin, Y., Yang, J. & Xiao, X. Latex-specific transcriptome analysis reveals mechanisms for latex metabolism and natural rubber biosynthesis in laticifers of *Hevea brasiliensis*. *Ind. Crops Prod.* **171**, 113835 (2021).
30. Yunyongwattanakorn, J., Tanaka, Y., Sakdapipanch, J. & Wongsasutthikul, V. Highly-purified natural rubber by saponification of latex: Analysis of residual protein in saponified natural rubber. *Rubber Chem. Technol.* **81**(1), 121–137 (2017).
31. Sabaei, A. A., Yusof, N. I. M., Napiah, M. & Sutanto, M. A review of using natural rubber in the modification of bitumen and asphalt mixtures used for road construction. *J. Teknologi* **81**(6), 81–88 (2019).
32. Svoboda, P. *et al.* Electron beam crosslinking of ethylene-octene copolymers. *Polymer* **81**, 119–128 (2015).
33. Morera, J. A., Verdejo, R., Manchado, M. A. L. & Santana, M. H. Sustainable mobility: The route of tires through the circular economy model. *Waste Manage.* **126**, 309–322 (2021).
34. Nicod, T. *et al.* Households' livelihood strategies facing market uncertainties: How did Thai farmers adapt to a rubber price drop?. *Agric. Syst.* **182**, 102846 (2020).
35. Kodsangma, A. *et al.* Effect of sodium benzoate and chlorhexidine gluconate on a biothermoplastic elastomer made from thermoplastic starch-chitosan blended with epoxidized natural rubber. *Carbohydr. Polymers* **242**, 116421 (2020).
36. Poongavalappil, S. *et al.* Cross-linking kinetics study and high temperature mechanical properties of ethylene-octene copolymer (EOC)/dicumyl peroxide (DCP) system. *Eur. Polymer J.* **47**, 1949–1955 (2011).
37. Tantala, J., Rachtanapun, C., Tongdeesontorn, W., Jantanasakulwong, K. & Rachtanapun, P. Moisture sorption isotherms and prediction models of carboxymethyl chitosan films from different sources with various plasticizers. *Adv. Mater. Sci. Eng.* **2019**, 4082439 (2019).
38. Saenjaiban, A. *et al.* Novel color change film as a time-temperature indicator using polydiacetylene/silver nanoparticles embedded in carboxymethyl cellulose. *Polymers* **12**(10), 2306 (2020).
39. Kasomo, R. M. *et al.* Selective flotation of rutile from almandine using sodium carboxymethyl cellulose (Na-CMC) as a depressant. *Miner. Eng.* **157**, 106544 (2020).
40. Klunklin, W. *et al.* Synthesis, characterization, and application of carboxymethyl cellulose from asparagus stalk end. *Polymers* **13**, 81 (2021).
41. Suriyatem, R. *et al.* Physical properties of carboxymethyl cellulose from palm bunch and bagasse agricultural wastes: Effect of delignification with hydrogen peroxide. *Polymers* **12**(7), 1505 (2020).
42. Rachtanapun, P. *et al.* Carboxymethyl bacterial cellulose from nata de coco: Effects of NaOH. *Polymers* **13**(3), 348 (2021).
43. Rachtanapun, P. *et al.* Effect of monochloroacetic acid on properties of carboxymethyl bacterial cellulose powder and film from nata de coco. *Polymers* **13**(4), 488 (2021).
44. Chaiwong, N. *et al.* Antioxidant and moisturizing properties of carboxymethyl chitosan with different molecular weights. *Polymers* **12**, 1445 (2020).
45. Jantanasakulwong, K. *et al.* Mechanical properties improvement of thermoplastic corn starch and polyethylene-grafted-maleic anhydride blending by Na⁺ ions neutralization of carboxymethyl cellulose. *Int. J. Biol. Macromol.* **120**, 297–301 (2018).
46. Khong, C. H., Lee, M. L. Y., Ahmad, I. & Phang, S. W. Development of grafted rubber/polyaniline/carboxymethyl cellulose film as green conductive polymer film. *Polymer Bull.* **2**, 2. <https://doi.org/10.1007/s00289-021-03689-8> (2021).
47. Supanakorn, G., Taokaew, S. & Phisalaphong, M. Ternary composite films of natural rubber, cellulose microfibril, and carboxymethyl cellulose for excellent mechanical properties, biodegradability and chemical resistance. *Cellulose* <https://doi.org/10.1007/s10570-021-04082-4> (2021).
48. Misman, M. A., Rashid, A. A. & Yahya, S. R. Modification and application of starch in natural rubber latex composites. *Rubber Chem. Technol.* **91**(1), 184–204 (2018).
49. Wang, J. & Li, S. Preparation and structure characterization of hydroxyethylmethacrylate grafted natural rubber latex. *Ind. Pract.* **24**(3), 283–290 (2014).
50. Aiello, P. B. *et al.* Evaluation of sodium diclofenac release using natural rubber latex as carrier. *Mater. Res.* **17**(1), 146–152 (2014).
51. Khanoonkon, N., Yoksan, R. & Ogale, A. A. Morphological characteristics of stearic acid-grafted starch compatibilized linear low density polyethylene/thermoplastic starch blown film. *Eur. Polymer J.* **76**, 266–277 (2016).
52. Abdullah, A. H. D., Chalimah, S., Primadona, I. & Hanantyo, M. H. G. Physical and chemical properties of corn, cassava, and potato starches. *IOP Conf. Ser. Earth Environ. Sci.* **160**(1), 012003 (2018).
53. Rozali, M. L. H., Ahmad, Z. & Isa, M. I. N. Interaction between carboxy methylcellulose and salicylic acid solid biopolymer electrolytes. *Adv. Mater. Res.* **1107**, 223–229 (2015).
54. Sharaf, S. & Hebeish, A. A. Novel nanocomposite hydrogel for wound dressing and other medical applications. *RSC Adv.* **5**, 103036 (2015).
55. Bao, W., Kossen, H., Richards, J. & Schneider, U. Catalytic and significant stoichiometric use of sodium species in molecular organic synthesis. *Catal. Earth-Abundant Elem.* **40**, 1–27 (2020).
56. Han, Y., Yu, J., Chen, T., Liu, X. & Sun, L. Study on catalytic pyrolysis mechanism of natural rubber (NR) over Zn-modified ZSM5 catalysts. *J. Energy Inst.* **94**, 210–221 (2021).
57. Zeng, Y. & Tang, A. Comparison of effects of basalt and polyacrylonitrile fibers on toughness behaviors of lightweight aggregate concrete. *Constr. Build. Mater.* **282**, 122572 (2021).
58. Tavares, K. M. *et al.* Effect of carboxymethyl cellulose concentration on mechanical and water vapor barrier properties of corn starch films. *Carbohydr. Polymers* **246**, 116521 (2020).
59. Tamiya, T. *et al.* Enhancement of interfacial adhesion in immiscible polymer blend by using a graft copolymer synthesized from propargyl-terminated poly(3-hydroxybutyrate-co-3-hydroxyhexanoate). *Eur. Polymer J.* **130**, 109662 (2020).
60. Igwe, I. O. & Ezeani, O. E. Studies on the transport of aromatic solvents through filled natural rubber. *Int. J. Polymer Sci.* **2012**, 212507 (2012).
61. Xiao, C. & Gao, Y. Preparation and properties of physically crosslinked sodium carboxymethylcellulose/poly(vinyl alcohol) complex hydrogels. *Appl. Polymer* **107**(3), 1568–1572 (2007).
62. Chujiang, C., Jinzhi, L., Zhigang, S., Shulin, M. & Yushan, X. Synthesis of hydrophobic corn starch with high flowability by surface modification. *Starch/Stärke* **61**, 344–351 (2009).
63. Vidal, R. R. L., Balaban, R. & Borsali, R. Amphiphilic derivatives of carboxymethylcellulose: evidence for intra- and intermolecular hydrophobic associations in aqueous solutions. *Polym. Eng. Sci.* **48**(10), 2011–2026 (2008).
64. Barbucci, R., Magnani, A. & Consumi, M. Swelling behavior of carboxymethylcellulose hydrogels in relation to cross-linking, pH, and charge density. *Macromolecules* **33**, 7475–7480 (2000).
65. Hesse, J. C., Schedel, M., Diedel, R. & Sass, I. Influence of swelling and non-swelling clays on the thermal properties of grouting materials for borehole heat exchangers. *Appl. Clay Sci.* **210**, 106154 (2021).
66. Zhu, B., Liu, J. & Gao, W. Process optimization of ultrasound-assisted alcoholic-alkaline treatment for granular cold water swelling starches. *Ultrason. Sonochem.* **38**, 579–584 (2017).

Acknowledgements

The authors gratefully acknowledge the Faculty of Agro-Industry, Chiang Mai University, for their support. This research was supported by the Program Management Unit for Human Resources & Institutional Development, Research and Innovation, Office of National Higher Education Science Research and Innovation Policy Council (Grant Number B16F640001). This research was partially supported by Chiang Mai University.

Author contributions

K.J., and N.L. designed the research study; K.J. prepared the sample and investigated; K.J., N.L., T.C., P.R., P.J., W.R., and P.S. contributed to data analysis; K.J., N.L., T.O., C.T., and S.R.S. discussed the results; K.J., N.L., Y.P., and S.T. were involved in drafting and editing of this work.

Competing interests

The authors declare no competing interests.

Additional information

Correspondence and requests for materials should be addressed to K.J.

Reprints and permissions information is available at www.nature.com/reprints.

Publisher's note Springer Nature remains neutral with regard to jurisdictional claims in published maps and institutional affiliations.



Open Access This article is licensed under a Creative Commons Attribution 4.0 International License, which permits use, sharing, adaptation, distribution and reproduction in any medium or format, as long as you give appropriate credit to the original author(s) and the source, provide a link to the Creative Commons licence, and indicate if changes were made. The images or other third party material in this article are included in the article's Creative Commons licence, unless indicated otherwise in a credit line to the material. If material is not included in the article's Creative Commons licence and your intended use is not permitted by statutory regulation or exceeds the permitted use, you will need to obtain permission directly from the copyright holder. To view a copy of this licence, visit <http://creativecommons.org/licenses/by/4.0/>.

© The Author(s) 2021, corrected publication 2021